Magnetic dichroism in angle-resolved hard x-ray photoemission from buried layers

Xeniya Kozina, Gerhard H. Fecher,* Gregory Stryganyuk, Siham Ouardi, Benjamin Balke, and Claudia Felser
Institut für Anorganische und Analytische Chemie, Johannes Gutenberg Universität, D-55099 Mainz, Germany

Gerd Schönhense
Institut für Physik, Johannes Gutenberg Universität, D-55099 Mainz, Germany

Eiji Ikenaga, Takeharu Sugiyama, Naomi Kawamura, and Motohiro Suzuki
Japan Synchrotron Radiation Research Institute, SPring-8, Hyogo 679-5198, Japan

Tomoyuki Taira, Tetsuya Uemura, and Masafumi Yamamoto
Division of Electronics for Informatics, Hokkaido University, Sapporo 060-0814, Japan

Hiroaki Sukegawa, Wenhong Wang, and Koichiro Inomata
National Institute for Materials Science, Tsukuba 305-0047, Japan

Keisuke Kobayashi
National Institute for Materials Science, SPring-8, Hyogo 679-5148, Japan
(Received 20 June 2011; published 15 August 2011)

This work reports the measurement of magnetic dichroism in angular-resolved photoemission from in-plane magnetized buried thin films. The high bulk sensitivity of hard x-ray photoelectron spectroscopy (HAXPES) in combination with circularly polarized radiation enables the investigation of the magnetic properties of buried layers. HAXPES experiments with an excitation energy of 8 keV were performed on exchange-biased magnetic layers covered by thin oxide films. Two types of structures were investigated with the IrMn exchange-biasing layer either above or below the ferromagnetic layer: one with a CoFe layer on top and another with a Co_2FeAl layer buried beneath the IrMn layer. A pronounced magnetic dichroism is found in the Co and Fe $2p$ states of both materials. The localization of the magnetic moments at the Fe site conditioning the peculiar characteristics of the Co_2FeAl Heusler compound, predicted to be a half-metallic ferromagnet, is revealed from the magnetic dichroism detected in the Fe $2p$ states.

DOI: 10.1103/PhysRevB.84.054449 PACS number(s): 75.25.−j, 79.60.−i, 85.75.−d, 71.20.Lp

I. INTRODUCTION

Rapid breakthroughs in the area of spintronics have led to the development of electronic devices with improved performance. Being a principal constituent part of such devices, complex multilayer structures have caused considerable interest in exploring their unique properties and at the same time have made this task rather sophisticated. Along with investigation of micromagnetic properties, an improved understanding of magnetoelectronic properties of deeply buried layers and interfaces in magnetic multilayer structures is of the most importance in the viewpoint of their potential applications in the field of magnetic recording, as data storage devices and sensors.

Magnetic circular dichroism (MCD) in photoabsorption and photoemission has become a very powerful tool for the element-specific investigation of the magnetic properties of alloys and compounds. Thus far, such studies have been mainly carried out using soft x-rays, resulting in a rather surface sensitive technique due to the low-electron mean free path of the resulting low-energy electrons. The application of hard x-rays[1] results in the emission of electrons with high kinetic energies and thus, it increases the probing depth.[2] The bulk sensitivity of this technique was recently proved and, for $h\nu > 8$ keV, the bulk spectral weight was found to reach more than 95%.[3] Hard X-ray photoelectron spectroscopy (HAXPES) has been found to be a well-adaptable non-destructive technique for the analysis of chemical and electronic states.[4,5] It was recently shown that HAXPES can be combined easily with variable photon polarization when using phase retarders.[6] Linear dichroism in the angular distribution of the photoelectrons is achieved using linearly polarized hard x-rays and is successfully applied to identify the symmetry of valence band states in Heusler compounds.[7] In combination with excitation by circularly polarized x-rays,[6] this method will serve as a unique tool for the investigation of the electronic and magnetic structure of deeply buried layers and interfaces.

Baumgarten *et al.*[8] carried out a pioneering study on magnetic dichroism in photoemission and observed this phenomenon in the core-level spectra of transition metals. The effect, however, was rather small (a few percentage points) because of the limited resolution of the experiment. It was later shown that dichroic effects are also obtained using linearly or even unpolarized photons.[9,10] The observed intensity differences in photoemission are essentially a phenomenon specific to angular-resolved measurements, and therefore, these have been termed as magnetic circular dichroism in the angular distribution (MCDAD).[11,12]

II. MAGNETIC DICHROISM IN THE ANGULAR DISTRIBUTION OF PHOTOELECTRONS MDAD

Theoretical atomic single-particle models were quite successful in describing, explaining, and predicting many aspects of magnetic dichroism. Cherepkov *et al.* elaborated the general formalism for the dichroism in photoemission excited by circularly, linearly, and unpolarized radiation.[11] They showed that MCDAD is very sensitive to the geometry of the experiment and depends strongly on the relative orientation between the magnetization, helicity, and momentum of the excited electrons. The maximum effect is obtained when the magnetization and helicity vectors are parallel; the effect decreases with an increase in the angle between these vectors.

The electronic states in solids usually do not carry a spherical or axial symmetry as in free atoms but have to follow the symmetry of the crystal.[13] The angular distribution $I^j(\mathbf{k},\mathbf{n})$ of the photoemitted electrons—as derived, for example, in Ref. 11 for the case of axially symmetric polarized atoms—has to account for the nondiagonal density matrix $\rho^{\mathbf{n}}_{NM'_N}$.[14] This leads to the following equation for the case of a nonaxial symmetry:

$$I^j(\mathbf{k},\mathbf{n}) = \frac{c_\sigma}{[l]}\sqrt{\frac{3\,[j]}{4\pi}}\sum_{\kappa,L}\sum_{N}[N]^{1/2}\,C^j_{\kappa LN}\sum_{x,M}\sum_{M_N,M'_N} \times \rho^{\gamma}_{\kappa x}\rho^{\mathbf{n}}_{NM'_N}(j)Y^*_{LM}(\mathbf{k})D^N_{M_NM'_N}(\Omega)\begin{pmatrix}\kappa & L & N\\ x & M & M_N\end{pmatrix}, \tag{1}$$

where l and j are the orbital and the total angular momentum of an electron in the initial state. $C^j_{\kappa LN}$ are the dynamic parameters derived from the radial matrix elements and $\rho^{\gamma}_{\kappa x}$ are photon state multipoles.[14] $D^j_{mm_j}(\Omega)$ is the Wigner rotation matrix with Ω being the set of Euler angles describing the rotation from the laboratory to the atomic coordinate frame. The direction of the electron momentum $\vec{k} = \mathbf{k}(\theta,\phi)$ is defined by the angles θ and ϕ (see Fig. 1). Finally, c_σ is a photon-energy-($h\nu$) dependent constant, $c_\sigma = \frac{4\pi^2\alpha\,h\nu}{3}$, where α is the fine structure constant.

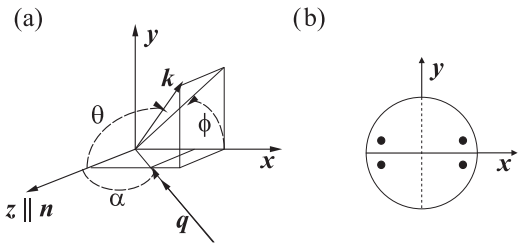

FIG. 1. (a) The coordinate system used for the investigation of photoemission. $\mathbf{k}(\theta,\phi)$ is the electron momentum, q is the photon beam and n is the principal axis of alignment. θ and ϕ are the angles defining the direction of the outgoing photoelectrons. α is the angle of photon incidence (in the x-z plane) as defined in optics. It is seen that the angle describing the photon propagation in spherical coordinates is given by $\Theta_q = \alpha + \pi$. The direction of the z axis corresponds to the quantization axis $\mathbf{n}$. (b) The direction of the in-plane axes x and y is illustrated for an object with C_{2v} symmetry.

TABLE I. State multipoles of $|L,J\rangle = |0,1/2\rangle$, $|1,1/2\rangle$, $|1,3/2\rangle$, and $|2,3/2\rangle$ states.

J	$\frac{1}{2}$		$\frac{3}{2}$			
M_J	$+\frac{1}{2}$	$-\frac{1}{2}$	$+\frac{3}{2}$	$+\frac{1}{2}$	$-\frac{1}{2}$	$-\frac{3}{2}$
ρ_{00}	$\frac{1}{\sqrt{2}}$	$\frac{1}{\sqrt{2}}$	$\frac{1}{2}$	$\frac{1}{2}$	$\frac{1}{2}$	$\frac{1}{2}$
ρ_{10}	$\frac{1}{\sqrt{2}}$	$-\frac{1}{\sqrt{2}}$	$\frac{3}{2\sqrt{5}}$	$\frac{1}{2\sqrt{5}}$	$-\frac{1}{2\sqrt{5}}$	$-\frac{3}{2\sqrt{5}}$
ρ_{20}	–	–	$\frac{1}{2}$	$-\frac{1}{2}$	$-\frac{1}{2}$	$\frac{1}{2}$
ρ_{30}	–	–	$\frac{1}{2\sqrt{5}}$	$-\frac{3}{2\sqrt{5}}$	$\frac{3}{2\sqrt{5}}$	$-\frac{1}{2\sqrt{5}}$

This formalism can also be used to consider open-shell atoms and the multiplets resulting from the interaction between the core states and the open-shell valence states. In that case, the dynamic parameters $C^j_{J\kappa LN}$ have to be calculated for the appropriate coupling scheme (jj, LSJ, or intermediate) with the single particle quantum numbers j,m being replaced by those (J,M) describing the complete atomic state.[11] In that case, the dynamic parameter will redistribute the single-electron results in a particular way over the states of a multiplet (see Refs. 15 and 16).

The state multipoles of the s, p, and d states that define the intensity and the sign and magnitude of the dichroism are summarized in Tables I and II. Note that the state multipoles are independent of the orbital angular momentum L, and they depend only on the total angular momentum J and its projection M_J.

A. MDAD equations for the grazing incidence geometry

In the following, let us consider the special case of geometry with the photons impinging in the x-z plane with unit vector of the photon momentum $\hat{q} = (-\cos(\alpha), -\sin(\alpha), 0)$. At such a grazing incidence with $\alpha = \pi/2$ it becomes $\hat{q} = (-1,0,0)$. The electrons are observed in the direction perpendicular to the photon beam ($\theta = \frac{\pi}{2} - \alpha$) with the momentum $\hat{k} = (-\sin(\theta), 0, \cos(\theta))$. At a photon incidence of $\alpha = \pi/2$ it becomes $\hat{k} = (0,0,1)$. (Compare also Figs. 1 and 3.)

Now examine the case: $\vec{n} \to -\vec{n}$ where the magnetic dichroism emerges from a switching of the direction of magnetization with the initial direction $\vec{n} = (1,0,0)$ that is along the x axis. Applying Eq. (1) and the state multipoles

TABLE II. State multipoles of $|L,J\rangle = |2,5/2\rangle$ states.

J	$\frac{5}{2}$					
M_J	$-\frac{5}{2}$	$-\frac{3}{2}$	$-\frac{1}{2}$	$+\frac{1}{2}$	$+\frac{3}{2}$	$+\frac{5}{2}$
ρ_{00}	$\frac{1}{\sqrt{6}}$	$\frac{1}{\sqrt{6}}$	$\frac{1}{\sqrt{6}}$	$\frac{1}{\sqrt{6}}$	$\frac{1}{\sqrt{6}}$	$\frac{1}{\sqrt{6}}$
ρ_{10}	$-\frac{5}{\sqrt{70}}$	$-\frac{3}{\sqrt{70}}$	$-\frac{1}{\sqrt{70}}$	$\frac{1}{\sqrt{70}}$	$\frac{3}{\sqrt{70}}$	$\frac{5}{\sqrt{70}}$
ρ_{20}	$\frac{5}{2\sqrt{21}}$	$-\frac{1}{2\sqrt{21}}$	$-\frac{2}{\sqrt{21}}$	$-\frac{2}{\sqrt{21}}$	$-\frac{1}{2\sqrt{21}}$	$\frac{5}{2\sqrt{21}}$
ρ_{30}	$-\frac{5}{6\sqrt{5}}$	$\frac{7}{6\sqrt{5}}$	$\frac{2}{3\sqrt{5}}$	$-\frac{2}{3\sqrt{5}}$	$-\frac{7}{6\sqrt{5}}$	$\frac{5}{6\sqrt{5}}$
ρ_{40}	$\frac{1}{2\sqrt{7}}$	$-\frac{3}{2\sqrt{7}}$	$\frac{1}{\sqrt{7}}$	$\frac{1}{\sqrt{7}}$	$-\frac{3}{2\sqrt{7}}$	$\frac{1}{2\sqrt{7}}$
ρ_{50}	$-\frac{1}{6\sqrt{7}}$	$\frac{5}{6\sqrt{7}}$	$-\frac{5}{3\sqrt{7}}$	$\frac{5}{3\sqrt{7}}$	$-\frac{5}{6\sqrt{7}}$	$\frac{1}{6\sqrt{7}}$

of Table I, the circular magnetic dichroism in the angular distribution for p states is given by the equations:

$$\begin{aligned}&\mathrm{CMDAD}^{\sigma+}(p)\\&\quad=-\rho_{10}\sin(\alpha)\left(\sqrt{\tfrac{2}{3}}C^{(1,0,1)}_{JkLN}+\sqrt{\tfrac{1}{15}}C^{(1,2,1)}_{JkLN}(1-6\cos^2(\alpha))\right)\\&\mathrm{CMDAD}^{\sigma-}(p)\\&\quad=+\rho_{10}\sin(\alpha)\left(\sqrt{\tfrac{2}{3}}C^{(1,0,1)}_{JkLN}+\sqrt{\tfrac{1}{15}}C^{(1,2,1)}_{JkLN}(1-6\cos^2(\alpha))\right)\end{aligned}\tag{2}$$

The circular magnetic dichroism in the angular distribution (CMDAD) for opposite helicity of the photons has an opposite sign. The equations for the $p_{1/2}$ and $p_{3/2}$ states are the same. The magnitude differs, however, because of the differences in the state multipoles ρ_{10} and dynamical parameters C_{JkLN}.

For $\alpha=\pi/2$ the CMDAD of the p states ($J=1/2,3/2$) becomes simply:

$$\mathrm{CMDAD}^{\sigma\pm}(p_J)=\mp\rho_{10}\left(\sqrt{\tfrac{2}{3}}C^{(1,0,1)}_{JkLN}+\sqrt{\tfrac{1}{15}}C^{(1,2,1)}_{JkLN}\right).\tag{3}$$

The linear counterpart LMDAD vanishes in that geometry, independent whether the photons are s or p polarized. At $\alpha=\pi/2$ the magnetic dichroism in the angular distribution vanishes for all p states independent of the polarization of the photons if the magnetization is perpendicular to the plane spanned by the photon incidence and the electron momentum [here for the x-z plane with $\vec{n}=(0,\pm1,0)$].

III. EXPERIMENTAL DETAILS

The present study reports on the MCDAD experiment in the HAXPES range on different types of exchange-biased structures with epitaxially grown ferromagnetic layers of CoFe and Co_2FeAl, these being typical materials used in tunnel magnetoresistive devices (see Fig. 2). The on-top approach multilayers were deposited in the sequence MgO(100) substrate/MgO buffer layer (10 nm)/$Ir_{78}Mn_{22}$ (10 nm)/CoFe (3 nm)/MgO barrier (2 nm)/AlO_x (1 nm)[17] that corresponds to the lower exchange-biased electrode of a magnetic tunnel junction (MTJ). After growth the stacks were annealed at 350 °C for 1 h in vacuum of 5×10^{-2} Pa in a magnetic field of 0.4 MAm^{-1} to provide exchange biasing of the CoFe layer film through the IrMn/CoFe interface (see also Ref. 18). The on-bottom configuration was realized in the multilayer sequence MgO(100) substrate/Cr buffer layer (40 nm)/Co_2FeAl (30 nm)/$Ir_{78}Mn_{22}$ (10 nm)/AlO_x (1 nm).[19] The sample stacks were annealed at 400 °C for 1 h in vacuum under a magnetic field of 0.4 MAm^{-1} to provide exchange biasing to the Co_2FeAl thin film through the Co_2FeAl/IrMn interface (see also Ref. 19). In both cases, the topmost AlO_x layers served as a protective coating. All metal layers were deposited by magnetron sputtering and electron beam evaporation was used to epitaxially grow the MgO barrier. IrMn serves as an exchange-biasing layer that keeps CoFe or Co_2FeAl magnetized in preset directions.

The magnetized samples were mounted pairwise with opposite magnetization on the same sampleholder and can be selected via sample shift. Care was taken that the magnetization directions were antiparallel and that surfaces were

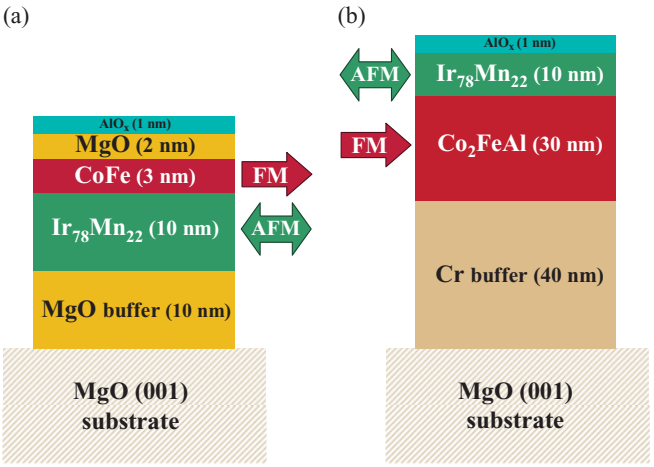

FIG. 2. (Color online) Sketch of the exchange-biased films used in the dichroism experiments. The multilayer structure in (a) corresponds to the lower part of the electrode and is realized in on-top configuration with CoFe ferromagnetic layer. The structure shown in (b) presents on-bottom configuration with Co_2FeAl ferromagnetic layer. In both films a 1-nm-thick AlO_x layer is used as a protective cap.

parallel to avoid different detection angles. The mounting of the samples at the fixed sample manipulator was chosen to have up/down as well as left/right pairs as it is shown in Fig. 3). This allowed to probe the dichroism by varying both the direction of magnetization and the direction of helicity.

The HAXPES experiments with an excitation energy of 7.940 keV were performed using beamline BL47XU at SPring-8.[20] The energy distribution of the photoemitted electrons was analyzed using a hemispherical analyzer (VG-Scienta R4000-12 kV) with an overall energy resolution of 150 or 250 meV. The angle between the electron spectrometer and the photon propagation was fixed at 90°. The detection angle was set to $\theta=2°$ in order to reach the near-normal emission geometry and to ensure that the polarization vector of the circularly polarized photons is nearly parallel (σ^-) or antiparallel (σ^+) to the in-plane magnetization M^+. The

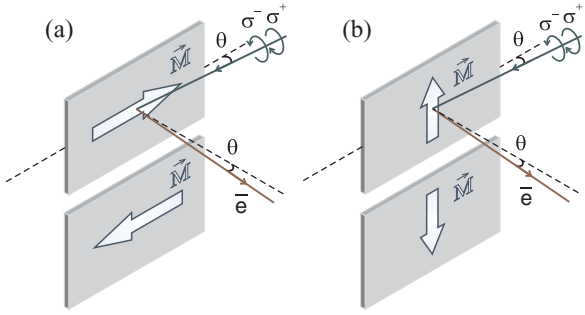

FIG. 3. (Color online) Scheme of the experimental geometry. The incidence angle θ (with respect to the surface plane) of the circularly polarized photons was fixed to 2°. X-rays of opposite helicity (σ^+ and σ^-) were provided by a phase retarder. Further, samples with opposite directions of magnetization are used. In (a) the in-plane magnetization **M** is nearly parallel to the beam axis and in (b) the in-plane magnetization is perpendicular to the beam axis. The electron detection is fixed and perpendicular to the photon beam.

sign of the magnetization was varied by mounting samples with opposite directions of magnetization (M^+, M^-). The polarization of the incident photons was varied using an in-vacuum phase retarder based on a 600-μm-thick diamond crystal with (220) orientation.[21] The direct beam is linearly polarized with $P_p = 0.99$. Using the phase retarder, the degree of circular polarization is set such that $P_c > 0.9$. The circular dichroism is characterized by an asymmetry that is defined as the ratio of the difference between the intensities I^+ and I^- and their sum, $A = (I^+ - I^-)/(I^+ + I^-)$, where I^+ corresponds to σ^+- and I^- to σ^-- type helicity. Magnetic dichroism may be defined in a similar manner using the differences in the intensities if the direction of the magnetization is changed keeping the polarization of the photons fixed.

The photon flux on the sample was about 10^{11} photons per second in a bandwidth of 10^{-5} during the measurements at the given excitation energy. The vertical spot size on the sample is 30 μm, while in horizontal direction, along the entrance slit of the analyzer, the spot was stretched to approximately 7 mm. The measurements were performed using grazing incidence geometry. The resulting count rates (taken from the equivalent gray scale values provided by the spectrometer software) were in the order of 0.6 to 6 MHz for the core level spectra, including shallow core levels and about 0.25 MHz for the valence band.

IV. RESULTS AND DISCUSSION

Figure 4 shows the $2p$ core-level spectra of Co that were taken from an exchange-biased CoFe film that was covered by oxide films. A pronounced difference was observed in the spectra taken with photons having opposite helicity for a fixed direction of magnetization. The pure difference $\Delta I = I^+ - I^-$ presented in the figure is already free of the influence of the background and gives the correct shape of the magnetic dichroism. This means that it contains all characteristic features of the magnetic dichroism. For

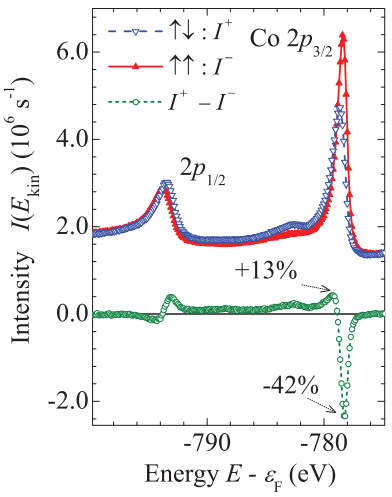

FIG. 4. (Color online) Polarization-dependent photoelectron spectra of the Co $2p$ core-level emission from CoFe on top of an IrMn exchange-biasing layer and the difference of two spectra. Asymmetry values are marked at selected energies.

quantification and comparison of the dichroic effects, the MCDAD asymmetry was determined from

$$A = \frac{(I^+ - I^-)}{(I^+ + I^-)} = \frac{\Delta I}{2I} \tag{4}$$

after subtracting a Shirley-type background from the spectra to find the asymmetry caused only by the direct transition. The background subtraction leads, however, to a very low intensity in the beginning, in the end of the spectral energy range as well as in the range between the spin-orbit split peaks in both spectra (that is in the ranges of the spectra where no signal from the transition itself is expected). This, in turn, leads to very high and rather nonphysical values of the calculated asymmetry in these energy ranges. From the above remark on ΔI it is, therefore, advantageous to show the differences of the intensities and to mark the asymmetry for characteristic energies only. Here the largest obtained asymmetry value is -42% at Co $2p_{3/2}$.

As one can see, the spin-orbit splitting of the Co $2p$ states is clearly resolved, as expected. When going from $p_{3/2}$ to $p_{1/2}$, the dichroism changes its sign across the $2p$ spectra in the sequence: $-\ +\ +\ -$; as appears characteristic of a Zeemann-type m_j sublevel ordering. This sequence of signs is directly expected from Eq. (3) and the state multipoles ρ_{10} given in Table I when identifying the states of the magnetically split $2p$ doublet as $|j,m_j\rangle$ in the single-particle description. The details of the MCDAD reveal, however, that the situation is more complicated. In particular, the dichroism in the Fe $2p$ spectra does not vanish in the region between the spin-orbit doublet. The multiplet formalism to describe the spectra in more detail will be given below.

MCDAD has previously been used to investigate the itinerant magnetism of ferromagnetic elements such as Co, Fe, and Ni, where it was explained in terms of single-particle models.[12,22–24] As demonstrated in the case of Ni, however, the single-particle approach poorly describes all the peculiarities of the complex spectra. van der Laan and Thole considered the MCDAD phenomenon by taking into account the influence of electron correlation effects in the frame of atomic many-particle models that were successfully used to describe both localized and itinerant magnetism phenomena.[11,15,24] Many-body effects play an important role when using polarized incident photons. The correlation between spin and orbital moments, $2p$ core-hole, and spin-polarized valence band results in a rich multiplet structure that spreads out over a wide energy range of a spectrum.[25] In strongly correlated systems, the bulk magnetic and electronic properties differ markedly from the surface ones. However, as observed previously, MCDAD with radiation in the soft x-ray range is highly sensitive to the surface where the dichroism is influenced by symmetry breaking.[26] Because of the strong inelastic electron scattering in this energy range, the escape depth of the photoemitted electrons of a few angstroms becomes comparable to the thickness of a monolayer. The tuning of the excitation energy also affects the photoionization cross sections. At high energies, the intensities from the d states of transition metals are reduced as compared to the partial cross sections of the s and p states.[2,27,28] The shape and magnitude of the asymmetry depend on the partial bulk to surface spectral

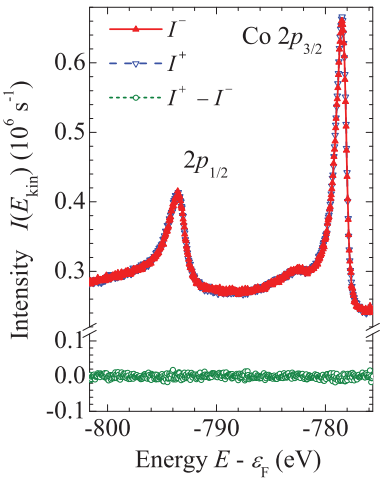

FIG. 5. (Color online) Illustration of the vanishing dichroism in photoemission when the photon polarization vector is perpendicular to the in-plane magnetization vector demonstrated for the Co $2p$ state of CoFe. Shown are the photoelectron spectra I^+, I^- and their difference $I^+ - I^-$ obtained with different helicity at fixed magnetization perpendicular to the photon beam.

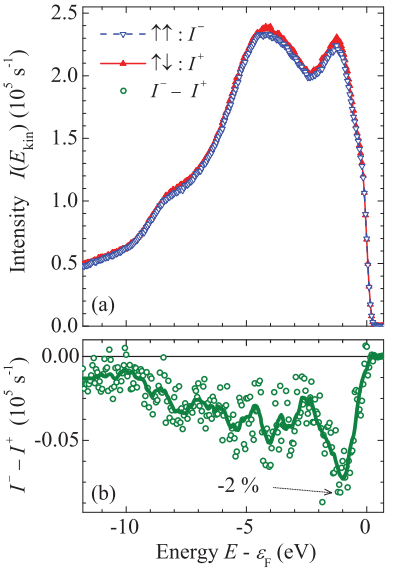

FIG. 6. (Color online) MCDAD in valence band of CoFe on top of IrMn. The asymmetry is given at −1 eV below Fermi level.

weights; hence, only at high energies, the dichroism effects appear to be related to the bulk properties.

It was carefully proven that the dichroism vanished in the geometry in which the projection of the photon vector is perpendicular to the magnetization, independently of whether the photon helicity or the magnetization was reversed. This indicates that the films are perfectly magnetized in the direction forced by the exchange-biasing layer magnetization. As an example, Fig. 5 confirms the absence of the dichroic signal at the Co $2p$ states of the CoFe film in agreement to the theoretical description given above.

Figure 6 shows the polarization dependence of the CoFe valence band spectra together with the resulting magnetic dichroism. The MCDAD observed for the valence band is much smaller as compared to the core-level photoemission. The largest asymmetry is approximately −2% at −1 eV below the Fermi energy. Such low asymmetry values were also observed when using low photon and kinetic energies.[29] Only for excitation close to threshold, higher asymmetries arise in the case of one-[30] and two-photon photoemission.[31] In the range of the valence states, the detection is further complicated by the signal from the underlying IrMn layer that does not contribute to the dichroism. Because of the thin layer of CoFe and the large escape depth of the nearly 8 keV fast electrons, the two layers cannot be distinguished in the valence band. It is worthwhile to note that the dichroic signal itself arises exclusively from the buried, ferromagnetic CoFe layer.

For studies aimed toward the development of novel devices, it is necessary to also detect the magnetic signal from deeply buried layers. To prove the reliability of the proposed method, experiments were also performed on samples in which the IrMn exchange-biasing layer was on top of the layer structure.

Figure 7 compares the MCDAD results for the shallow core levels of CoFe in the on-top configuration [Fig. 7(a)] and the deeply buried Co_2FeAl in the on-bottom configuration beneath a 10-nm-thick IrMn film [Fig. 7(b)]. For such complex multilayer structures, the situation becomes complicated in that the signals from all the elements contained in the system are detected. In both cases the shallow core levels of all elements of the multilayers are detected. The intensity differences between Fe and Co $3p$ emission or Ir $4f$ and Mn $3p$ in the different configurations are obvious and arise from the damping of the intensity when the electrons pass through the layers above the emitting layer. Strong signals are still detected from the buried elements even though the ferromagnetic Co_2FeAl layer lies 10 nm beneath the antiferromagnetic IrMn layer, as is clearly seen in the inset of Fig. 7(b). A large asymmetry is clearly observed at the Co and Fe signals, and these are the ones responsible for the ferromagnetic properties

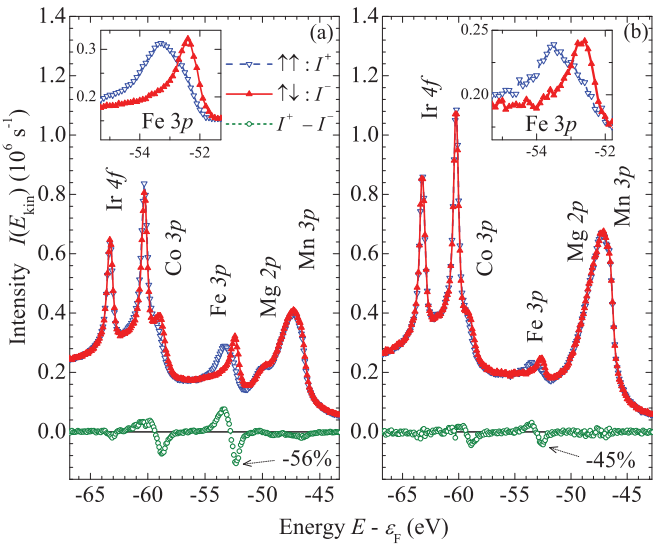

FIG. 7. (Color online) MCDAD for the shallow core level spectra obtained from the buried CoFe on top and Co_2FeAl beneath a 10-nm-thick IrMn film. The insets show an enlarged view of the Fe $3p$ states.

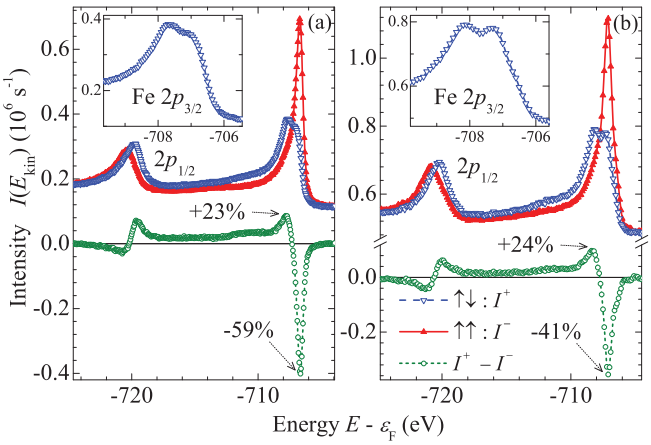

FIG. 8. (Color online) Polarization-dependent photoelectron spectra of the Fe $2p$ core-level emission from CoFe on top of an IrMn exchange-biasing layer, Co_2FeAl beneath IrMn and the corresponding differences of the spectra taken with the opposite helicity of light. Asymmetry values are marked at selected energies. The insets show an enlarged view of I^+ at the Fe $2p_{3/2}$ states in both cases.

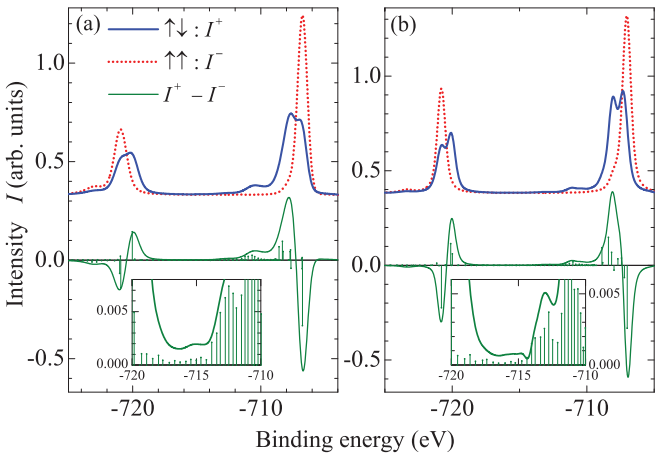

FIG. 9. (Color online) Calculated polarization-dependent photoelectron spectra of the Fe $2p$ core-level emission obtained by means of atomic multiplet calculations and their difference for CoFe (a) and Co_2FeAl (b). The insets show the enlarged views of the difference curve in the region between spin-orbitally split components of Fe $2p$ states. The bars mark the multiplet states.

of the system. The asymmetries of -56% (CoFe) and -45% (Co_2FeAl) in the Fe $3p$ signal are quite evident. In Co $3p$, it is well detected even though the direct spectra overlap with the Ir $4f$ states.

Figure 8 shows the polarization dependent HAXPES spectra and the MCDAD at the Fe $2p$ states of the buried CoFe (a) and Co_2FeAl (b) layers. The multiplet splitting at the Fe $2p_{3/2}$ is very well resolved and the MCDAD is well detected in both materials. The emission from the Co_2FeAl has a lower intensity and the resolution was therefore reduced to 250 meV in order to keep the counting rates comparable to those of the CoFe measurements. (Note that this does not influence the spectra much as they are governed by a lifetime broadening that is in the same order of magnitude.) It was shown [32] that linear magnetic dichroism (LMDAD) along with the circular one can be successfully applied to investigate the electronic and magnetic properties of surfaces and interfaces. The LMDAD asymmetry observed at Fe $2p_{3/2}$, however, was only at most -9% for a low excitation energy. In our studies the maximum asymmetries are -59% for CoFe and -41% for Co_2FeAl at Fe $2p_{3/2}$, and this is ideal for the analysis of the magnetic properties.

Closer inspection of the MCD spectra [see insets of Figs. 8(a) and 8(b)] reveals a striking distinction between the Fe $2p$ spectra of the two layer systems. Even though taken with a slightly lower resolution, the multiplet splitting of the Fe $2p_{3/2}$ emission from Co_2FeAl appears more pronounced as compared to the corresponding spectrum from CoFe. The mean splitting ΔE of the Fe $2p_{3/2}$ states is 0.8 and 1.0 eV for CoFe and Co_2FeAl, respectively. Co_2FeAl is supposed to be a half-metallic ferromagnet with a magnetic moment of 5 μ_B in the primitive cell and about 2.8 μ_B per Fe atom,[33] whereas CoFe is a regular band ferromagnet with a very high magnetic moment (about 2.5 μ_B at Fe).[34] In both cases the Fe moment is clearly above that of pure Fe (2.1 μ_B). One of the major differences is the localized magnetic moment of Fe in Co_2FeAl that is caused by a strong localization of the t_{2g} bands. In the ordered case of both compounds, the Fe atoms are in a cubic environment and are surrounded by 8 Co atoms. Co_2FeAl forms a perfect 2^3 CsCl supercell with every second Fe atom of CoFe replaced by Al. This causes additional Co-Al bonds that reduce the Co-Fe d-state overlap. The result is a localized moment at the Fe sites. From this viewpoint, Fe in Co_2FeAl is in closer to an covalent than a metallic state. For the Fe atoms, this causes a more pronounced interaction of the core hole at the ionized $2p$ shell with the partially filled $3d$ valence shell.

As mentioned above, the single-particle theory cannot explain the details of the spectra and their dichroism. It is necessary to respect the coupling between the ionized core and open valence shells. In the present case, this is the interaction between the $2p^5$ core hole and the open $3d$ valence shell of Fe. Therefore, multiplet calculations were carried out to explain the experimentally obtained results for the two different materials. They were performed by means of the charge transfer multiplet calculations for x-ray absorption spectroscopy (CTM4XAS)5.2 program,[35] using its x-ray photoelectron spectroscopy (XPS) option. The results are shown in Fig. 9. The simulations were made for a Fe^{3+} ionic ground state with $4s^0 3d^5$ configuration that describes well the emission from the Fe-$2p$ states of both systems, CoFe and Co_2FeAl. The Slater integrals (F_{dd}, F_{pd}, and G_{pd}) were reduced to 0.65; 0.55; 0.65 and 0.7; 0.5; and 0.5 of the free atom values to describe the spectra of CoFe and Co_2FeAl, respectively. As exchange interaction plays an important role in ferromagnetic materials, the effect of exchange splitting was taken into account by setting the magnetic splitting parameter M to 50 meV for CoFe and 450 meV for Co_2FeAl. The obtained values for the splitting ΔE of the Fe $2p_{3/2}$ states are 0.9 and 1.1 eV for CoFe and Co_2FeAl, respectively. The applied parameters resulted in a quite good agreement between calculated and experimental spectra and dichroism. Possible, slight disagreements may be attributed to the fact that the observed spectra depend on the degree of localization

or itineracy of the magnetic moment at the Fe site through the coupling of the $2p^5$ core hole with the d-valence bands. Fractional d-state occupancies (for example, $d^{5+x}, 0 < x < 1$) that might better describe the partial delocalization of d electrons of Fe in metallic systems, however, are not available in the atomic model. The insets in Fig. 9 present a enlarged view of the region of the dichroism between the main lines of the multiplet. In those insets one clearly recognizes the appearance of multiplet states over the entire energy range. These states form the characteristic structure of the dichroism that is in a good agreement with the experiment.

It is worthwhile to note that such differences in the multiplett structure of two very similar alloys are not resolved by X-ray circular dichroism (XMCD) in soft x-ray photo absorption.[36] This is found easily if comparing the here shown photoelectron spectra and dichroism to previously reported XMCD spectra of Fe containing Heusler compounds[37–39] where the XMCD spectra and dichroism appear rather without any resolved splitting of the $L_{2;3}$ lines.

V. SUMMARY AND CONCLUSIONS

In summary, MCDAD in hard x-ray photoelectron spectroscopy was used to study the magnetic response of the core level of buried, remanently magnetized layers. Using bulk-sensitive HAXPES-MCDAD, it was shown that IrMn exchange-biasing layers keep thin films of CoFe or Co_2FeAl remanently magnetized in a well-defined direction. Dichroism in the valence band spectroscopy is complicated in metal/metal layers; however, the situation will improve in metal/insulator structures in which the insulator does not contribute to the states at the Fermi energy.[4] The magnetic dichroism from core levels, including shallow core levels, of CoFe and buried Co_2FeAl multilayer has asymmetries up to above 58% when it is excited by circularly polarized hard x-rays and is thus much larger compared to that in the case of excitation by soft x-rays. As a noteworthy result, the differences in the Fe $2p$ emission from a regular ferromagnet (CoFe) and a suggested half-metallic ferromagnet (Co_2FeAl) were demonstrated. The splitting observed in Co_2FeAl points to the covalent character of the compound.

Overall, the high bulk sensitivity of HAXPES combined with circularly polarized photons will have a major impact on the study of the magnetic phenomena of deeply buried magnetic materials. The combination with recently proposed standing wave methods[40,41] will allow an element-specific study of the magnetism of buried layers and make feasible the investigation of the properties of magnetic layers not only at the surface but also at buried interfaces.

ACKNOWLEDGMENTS

Financial support by Deutsche Forschungsgemeinschaft and the Strategic International Cooperative Program of JST (DFG-JST: FE633/6-1) is gratefully acknowledged. We are thankful to the Japan Synchrotron Radiation Research Institute (JASRI) for the support of experiments within the approved 2009B0017 proposal. The team of Hokkaido University acknowledges the support of MEXT, Japan (Grants-in-Aid 20246054, 21360140, and 19048001) X.K. acknowledges the support of MAINZ.

*fecher@uni-mainz.de

[1] I. Lindau, P. Pianetta, S. Doniach, and W. E. Spicer, Nature **250**, 214 (1974).
[2] K. Kobayashi *et al.*, Appl. Phys. Lett. **83**, 1005 (2003).
[3] S. Suga and A. Sekiyama, Eur. Phys. J. Special Topics **169**, 227 (2009).
[4] G. H. Fecher *et al.*, Appl. Phys. Lett. **92**, 193513 (2008).
[5] X. Kozina, S. Ouardi, B. Balke, G. Stryganyuk, G. H. Fecher, C. Felser, S. Ikeda, H. Ohno, and E. Ikenaga, Appl. Phys. Lett. **96**, 072105 (2010).
[6] S. Ueda *et al.*, Appl. Phys. Exp. **1**, 077003 (2008).
[7] S. Ouardi *et al.*, Phys. Rev. Lett. **107**, 036402 (2011).
[8] L. Baumgarten, C. M. Schneider, F. Schäfers, H. Petersen, and J. Kirschner, Phys. Rev. Lett. **65**, 492 (1990).
[9] D. Venus, Phys. Rev. B **48**, 6144 (1993).
[10] M. Getzlaff, C. Ostertag, G. H. Fecher, N. A. Cherepkov, and G. Schönhense, Phys. Rev. Lett. **73**, 3030 (1994).
[11] N. A. Cherepkov, V. V. Kuznetsov, and V. A. Verbitskii, J. Phys. B **28**, 1221 (1995); G. van der Laan and B. T. Thole, Phys. Rev. B **52**, 15355 (1995).
[12] F. U. Hillebrecht, C. Roth, H. B. Rose, W. G. Park, E. Kisker, and N. A. Cherepkov, Phys. Rev. B **53**, 12182 (1996).
[13] G. H. Fecher, V. V. Kuznetsov, N. A. Cherepkov, and G. Schönhense, J. Electron Spectrosc. Relat. Phenom. **122**, 157 (2002).
[14] K. Blum, *Density Matrix Theory and Application* (Plenum, New York, 1981).
[15] B. T. Thole and G. van der Laan, Phys. Rev. Lett. **67**, 3306 (1991); Phys. Rev. B **44**, 12424 (1991); **50**, 11474 (1994); **49**, 9613 (1994).
[16] G. H. Fecher, J. Electron Spectrosc. Relat. Phenom. **114–116**, 1165 (2001).
[17] M. Masuda, T. Uemura, K. I. Matsuda, and M. Yamamoto, IEEE Trans. Magn. **44**, 3996 (2008).
[18] T. Marukame, T. Ishikawa, S. Hakamata, K. I. Matsuda, T. Uemura, and M. Yamamoto, Appl. Phys. Lett. **90**, 012508 (2007).
[19] W. Wang, H. Sukegawa, R. Shan, S. Mitani, and K. Inomata, Appl. Phys. Lett. **95**, 182502 (2009).
[20] K. Kobayashi, Nucl. Instrum. Methods A **601**, 32 (2009).
[21] M. Suzuki, N. Kawamura, M. Mizukami, A. Urata, H. Maruyama, S. Goto, and T. Ishikawa, Jpn. J. Appl. Phys. **37**, L1488 (1998).
[22] J. G. Tobin, K. W. Goodman, F. O. Schumann, R. F. Willis, J. B. Kortright, J. D. Denlinger, E. Rotenberg, A. Warwick, and N. V. Smith, Surf. Sci. **395**, L227 (1998).
[23] J. Henk, A. M. N. Niklasson, and B. Johansson, Phys. Rev. B **59**, 13986 (1999).
[24] J. Bansmann, L. Lu, K. H. Meiwes-Broer, T. Schlathölter, and J. Braun, Phys. Rev. B **60**, 13860 (1999); G. van der Laan and B. T. Thole, *ibid.* **48**, 210 (1993). .
[25] G. van der Laan, S. S. Dhesi, and E. Dudzik, Phys. Rev. B **61**, 12277 (2000).
[26] G. H. Fecher, Europhys. Lett. **29**, 605 (1995).
[27] G. Panaccione *et al.*, J. Phys. Condens. Matter **17**, 2671 (2005).

[28]G. H. Fecher, B. Balke, S. Ouardi, C. Felser, G. Schönhense, E. Ikenaga, J.-J. Kim, S. Ueda, and K. Kobayashi, J. Phys. D: Appl. Phys. **40**, 1576 (2007).
[29]D. Venus, Phys. Rev. B **56**, 2661 (1997).
[30]T. Nakagawa and T. Yokoyama, Phys. Rev. Lett. **96**, 237402 (2006).
[31]K. Hild, J. Maul, G. Schönhense, H. J. Elmers, M. Amft, and P. M. Oppeneer, Phys. Rev. Lett. **102**, 057207 (2009).
[32]G. Rossi, G. Panaccione, F. Sirotti, S. Lizzit, A. Baraldi, and G. Paolucci, Phys. Rev. B **55**, 11488 (1997).
[33]S. Wurmehl S. Wurmehl, G. H. Fecher, K. Kroth, F. Kronast, H. A. Dürr, Y. Takeda, Y. Saitoh, K. Kobayashi, H.-J. Lin, G. Schönhense, and C. Felser, J. Phys. D: Appl. Phys. **39**, 803 (2006).
[34]R. Richter and H. Eschrig, J. Phys. F **18**, 1813 (1988).
[35]E. Stavitski and F. M. F. de Groot, Micron **41**, 687 (2010).
[36]C. T. Chen, F. Sette, Y. Ma, and S. Modesti, Phys. Rev. B **42**, 7262 (1990); C. T. Chen, Y. U. Idzerda, H.-J. Lin, N. V. Smith, G. Meigs, E. Chaban, G. H. Ho, E. Pellegrin, and F. Sette, Phys. Rev. Lett. **75**, 1 (1995).
[37]H. J. Elmers, G. H. Fecher, D. Valdaitsev, S. A. Nepijko, A. Gloskovskii, G. Jakob, G. Schönhense, S. Wurmehl, T. Block, C. Felser, P.-C. Hsu, W.-L. Tsai, and S. Cramm, Phys. Rev. B **67**, 104412 (2003). H. J. Elmers, S. Wurmehl, G. H. Fecher, G. Jakob, C. Felser and G. Schönhense Appl. Phys. A **79**, 557 (2004).
[38]C. Felser, B. Heitkamp, F. Kronast, D. Schmitz, S. Cramm, H. A. Dürr, H.-J. Elmers, G. H. Fecher, S. Wurmehl, T. Block, D. Valdaitsev, S. A. Nepijko, A. Gloskovskii, G. Jakob, G. Schönhense, and W. Eberhardt, J. Phys.: Condens. Matter **15**, 7019 (2003).
[39]S. Wurmehl, G. H. Fecher, H. C. Kandpal, V. Ksenofontov, C. Felser, H.-J. Lin, and J. Morais, Phys. Rev. B **72**, 184434 (2005); S. Wurmehl, G. H. Fecher, H. C. Kandpal, V. Ksenofontov, C. Felser, and H.-J. Lin, Appl. Phys. Lett. **88**, 032503 (2006); S. Wurmehl, G. H. Fecher, K. Kroth, F. Kronast, H. A. Dürr, Y. Takeda, Y. Saitoh, K. kobayshi, H.-J. Lin, G. Schönhense, C. Felser, J. Phys. D: Appl. Phys. **39**, 803 (2006).
[40]C. S. Fadley, J. Electron Spectrosc. Relat. Phenom. **178–179**, 232 (2010).
[41]J. Zegenhagen, B. Detlefs, T.-L. Lee, S. Thiess, H. Isern, L. Petit, L. Andre, J. Roy, Y. Mi, and I. Joumard, J. Electron Spectrosc. Relat. Phenom. **178-179**, 258 (2010).